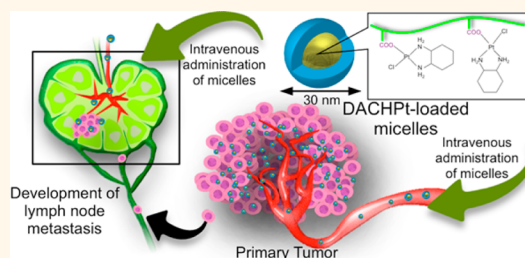# Systemic Targeting of Lymph Node Metastasis through the Blood Vascular System by Using Size-Controlled Nanocarriers

Horacio Cabral,[†] Jun Makino,[‡] Yu Matsumoto,[‡] Peng Mi,[§] Hailiang Wu,[†] Takahiro Nomoto,[§] Kazuko Toh,[‡] Naoki Yamada,[||] Yuriko Higuchi,[⊥] Satoshi Konishi,[#] Mitsunobu R. Kano,[▽] Hiroshi Nishihara,[○] Yutaka Miura,[‡] Nobuhiro Nishiyama,[§] and Kazunori Kataoka[*,†,‡,||,¶]

[†]Department of Bioengineering, Graduate School of Engineering, The University of Tokyo, 7-3-1 Hongo, Bunkyo-ku, Tokyo 113-8656, Japan, [‡]Center for Disease Biology and Integrative Medicine, Graduate School of Medicine, The University of Tokyo, 7-3-1 Hongo, Bunkyo-ku, Tokyo 113-0033, Japan, [§]Polymer Chemistry Division, Chemical Resources Laboratory, Tokyo Institute of Technology, R1-11, 4259 Nagatsuta, Midori-ku, Yokohama 226-8503, Japan, [||]Department of Materials Engineering, Graduate School of Engineering, The University of Tokyo, 7-3-1 Hongo, Bunkyo-ku, Tokyo 113-8656, Japan, [⊥]Graduate School of Pharmaceutical Sciences, Kyoto University, Yoshida-shimoadachi, Sakyo-ku, Kyoto 606-8501, Japan, [#]Department of Mechanical Engineering, Ritsumeikan University, Noji-higashi, Kusatsu, Shiga 525-8577, Japan, [▽]Department of Pharmaceutical Biomedicine, Graduate School of Medicine, Dentistry, and Pharmaceutical Sciences, Okayama University, 1-1-1 Tsushima-naka, Kita-ku, Okayama 700-8530, Japan, [○]Laboratory of Translational Pathology, Hokkaido University School of Medicine, North 15, West 7, Kita-ku, Sapporo 060-8638, Japan, and [¶]Innovation Center of NanoMedicine, 3-25-14, Tonomachi, Kawasaki-ku, Kawasaki 210-0821, Japan

ABSTRACT Occult nodal metastases increase the risk of cancer recurrence, demoting prognosis and quality of life of patients. While targeted drug delivery by using systemically administered nanocarriers can potentially control metastatic disease, lymph node metastases have been mainly dealt by locally injecting nanocarriers, which may not always be applicable. Herein, we demonstrated that sub-50 nm polymeric micelles incorporating platinum anticancer drugs could target lymph node metastases in a syngeneic melanoma model after systemic injection, even after removing the primary tumors, limiting the growth of the metastases. By comparing these micelles with clinically used doxorubicin-loaded liposomes (Doxil) having 80 nm, as well as a 70 nm version of the micelles, we found that the targeting efficiency of the nanocarriers against lymph node metastases was associated with their size-regulated abilities to extravasate from the blood vasculature in metastases and to penetrate within the metastatic mass. These findings indicate the potential of sub-50 nm polymeric micelles for developing effective conservative treatments against lymph node metastasis capable of reducing relapse and improving survival.

Metastasis to lymph nodes is a frequent clinical event for several tumors[1] and a central problem for the management of cancer, which is strongly associated with disseminated disease and poor prognosis.[2] Although surgery and radiation therapy are common treatments for removing lymph node metastasis with curative intent,[2] such approaches are associated with lymphedema, pain and prolonged hospitalization, while residual metastasis lead to recurrence of the disease.[3,4] Moreover, despite systemic chemotherapy has demonstrated complete responses in lymph node metastasis,[5,6] the poor access and short-lived concentration of chemotherapeutics within metastatic lymph nodes compels to use high doses, increasing the risk of dose-limiting toxicities, while subtherapeutic drug levels yields tumor reemergence and resistance to therapy.[7] Therefore, targeted delivery of chemotherapy to metastatic lymph nodes presents a promising approach for improving treatment efficacy, as well as prognosis and quality of life of patients.

Nanoscaled carriers are being used for selectively delivering chemotherapeutic agents to solid tumors after systemic administration, thus, enhancing the efficacy of therapies and

reducing the side effects of incorporated drugs.[8−10] In this way, systemically injected nanocarriers could offer substantial advantage for targeting lymph node metastasis, as any metastatic lymph node may be plausible for therapy regardless of the anatomical position. However, selective accumulation of nanocarriers in lymph node metastasis after systemic injection has been elusive so far, with current nanoparticle approaches also accumulating in healthy lymph nodes due to their lymphotropic mechanism, which is based on tissue extravasation, uptake by lymphatic vessels or macrophages, and migration to draining lymph nodes.[11,12] Besides, such mechanism is not suitable for targeting cytotoxic drugs due to the underlying risk of side effects, as well as the reduced accumulation in metastatic lymph nodes because of the impaired lymphatic drainage in tumors.[13] Therefore, present strategies for nanocarrier delivery to lymph node metastasis involve intralymphatic or local administration of carriers,[2,14−18] which are also limited by unpredictable or heterogeneous patterns of drainage,[19] occurrence of metastases in multiple nodes,[20] drainage to several nodal basins,[20] unknown primary sites,[21] obstruction of lymphatic flow,[22] or metastasis in lymph nodes beyond surgical area.[23] In view of these issues, systemic targeting of lymph node metastases by nanocarriers capable of reaching the metastasis through the blood vascular route could provide an effective modality against the whole metastatic setting.

Polymeric micelles, *i.e.*, self-assembled nanocarriers consisting of a drug-loaded hydrophobic core and poly(ethylene glycol) (PEG) hydrophilic shell, present exceptional tunable features for overcoming *in vivo* barriers en route to their biological targets after intravenous injection, including their relatively small size, prolonged blood circulation, and effective accumulation and penetration in solid tumors.[10,24] Thus, several micelle formulations loading anticancer agents are showing enhanced therapeutic responses with prolongation of survival rates and diminution of side effects in human clinical trials.[25−28] Among them, polymeric micelles with 30 nm diameter loading the parent complex of oxaliplatin, that is, (1,2-diaminocyclohexane)platinum(II) (DACHPt), have shown suppression of nodal metastases of scirrhous gastric cancer after intravenous injection.[29] Therefore, in this study, we elucidated the targeting mechanism of DACHPt-loaded micelles against lymph node metastases

by using a melanoma model, as melanoma invasion to lymph nodes is common in the clinic,[20,21,30] while it allow us to isolate the metastases by resecting the primary tumor. Moreover, the targeting ability of DACHPt/m was compared with that of clinically used PEGylated liposomes incorporating doxorubicin (Doxil), as liposomal nanocarriers have shown limited accumulation in metastatic lymph nodes after intravenous injection,[31,32] as well as with that of a 70 nm version of DACHPt/m,[33] which has comparable size to Doxil. Our results demonstrated that intravenously injected 30 nm DACHPt/m selectively accumulated in lymph node metastasis through the extravasation from the blood vascular compartment into the metastatic foci, and denoted the significance of the control of the size of the nanocarriers for the success of this process.

RESULTS AND DISCUSSION

Systemically Injected DACHPt/m Inhibited the Growth of Primary Orthotopic Melanoma and Its Lymph Node Metastases. DACHPt/m self-assembled in water due to the complex formation of the platinum drug with the carboxylate groups of the poly(glutamic acid) block of poly-(ethylene glycol)-*b*-poly(glutamic acid) [PEG-*b*-P(Glu)] copolymer.[34] We have previously demonstrated that DACHPt/m can maintain their micelle form during their extended life in the bloodstream[33−35] and reach deep tumor regions, even in poorly permeable tumors,[33] due to their relatively small diameter of 30 nm, leading to higher activity than free oxaliplatin in various tumors.[29,33,35,36] Herein, we initially evaluated the activity of DACHPt/m with 30 nm diameter (Table 1) and free oxaliplatin against primary melanoma tumors, which were prepared by inoculating highly metastatic murine melanoma B16-F10 cells expressing luciferase (B16-F10-luc) in the forepaw of mice. The size of the tumors was measured by using a caliper, starting the experiment when the tumors were 3 mm in diameter. While oxaliplatin, which was intravenously injected at its maximum tolerated dose (MTD), *i.e.*, 8 mg/kg, 3 times every second day (days 0, 2 and 4) failed to suppress the growth of primary tumors (Figure 1A), DACHPt/m at its MTD, 3 mg/kg in a similar dosing schedule, effectively limited the progression of the tumors (Figure 1A), without any body weight loss (Figure 1B).

Because B16-F10-luc tumors inoculated in the forepaw of mice spontaneously develop bioluminescent

TABLE 1. Size and Surface Charge of DACHPt-Loaded Micelles (DACHPt/m) with 30 and 70 nm Diameter and Doxil

nanocarrier	diameter (nm)[a]	polydispersity index[b]	number mean diameter by TEM (nm)[c]	volume mean diameter by TEM (nm)[c]	zeta potential (mV)[d]
30 nm DACHPt/m	30 ± 2	0.10	16	24	−0.5 ± 0.2
70 nm DACHPt/m	73 ± 1	0.07	52	61	−3.1 ± 1.3
Doxil	80 ± 1	0.06	76	79	0.0 ± 0.3

[a] Volume size distribution determined by dynamic light scattering (n = 3; mean ± SD). [b] Determined by dynamic light scattering. [c] Calculated by measuring the diameter of 100 particles. [d] Determined by laser Doppler electrophoresis at pH 7.4 (n = 4; mean ± SD).
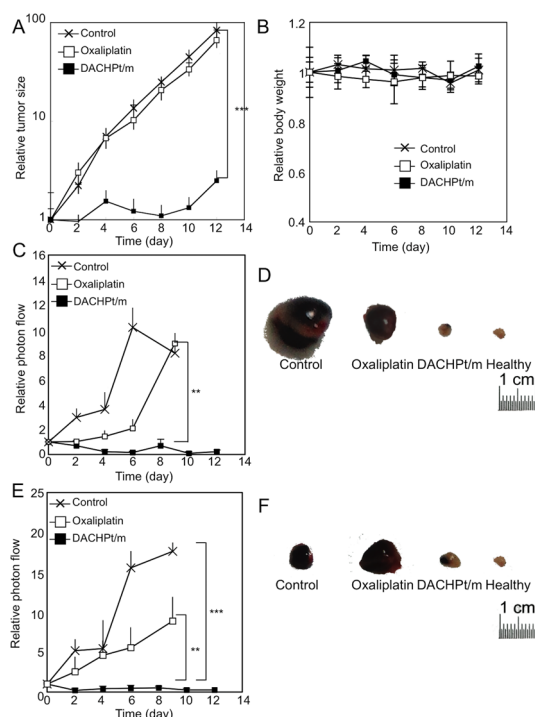
Figure 1. Antitumor activity of DACHPt-loaded micelles (DACHPt/m) against primary and metastatic tumors. (A) Relative size of primary tumors in the forepaw. Mice ($n = 5$) received saline, oxaliplatin at 8 mg/kg or DACHPt/m at 3 mg/kg on days 0, 2, and 4. Data presented as mean ± SEM ($n = 5$). **(B)** Relative body weight of mice during the antitumor activity experiment. Data presented as mean ± SD ($n = 5$). **(C)** Relative photon flow from lymph node metastasis in mice having primary tumors. Data presented as mean ± SEM ($n = 5$). **(D)** *Ex vivo* macroscopy of representative metastatic lymph nodes after 10 days of treatment in mice having primary tumors. **(E)** Relative photon flow from lymph node metastasis in mice with resected primary tumors. Data presented as mean ± SEM ($n = 5$). **(F)** *Ex vivo* macroscopy of representative metastatic lymph nodes after 10 days of treatment in mice with resected primary tumors. Mice ($n = 5$) received saline, oxaliplatin at 8 mg/kg or DACHPt/m at 3 mg/kg on days 0, 2, and 4. **$p < 0.05$; ***$p < 0.001$ determined by ANOVA with Tukey's multiple comparison test.

metastases in the brachial lymph nodes (Supporting Information Figure S1), the formation of metastases was daily followed by bioluminescent imaging the flank of mice. When the bioluminescent signal of the metastases became detectable, the size of the metastases was approximately 200 μm, as confirmed by histology (Supporting Information Figure S1). At this point, oxaliplatin and DACHPt/m were intravenously injected following the same dosing schedule used for orthotopic tumors, and the growth of the metastases was followed every 2 days by *in vivo* bioluminescence imaging. Micelles were again more efficacious than oxaliplatin, effectively reducing the growth of the metastases (Figure 1C). The superior activity of the micelles was visually confirmed after collecting metastatic lymph nodes 15 days after treatment with saline, oxaliplatin and DACHPt/m (Figure 1D).

Because the efficacy of the drugs against lymph node metastasis in the above-mentioned experiment

can be attributed not only to their activity against the metastatic foci, but also to their effect in primary tumors, we surgically removed the primary tumors in the forepaw after detecting the bioluminescent signal in the lymph nodes. Moreover, by eliminating the primary tumors, the lymphatic drainage of micelles from tumor tissues into metastatic lymph nodes *via* afferent lymphatic vessels was hindered, implying that the efficacy of systemically injected micelles can be associated with their direct accumulation in the metastases through the blood supply. Thus, 24 h after resection of primary tumors, the sole presence of metastasis was confirmed by *in vivo* bioluminescence imaging, and the efficacy of oxaliplatin and DACHPt/m was evaluated by imaging the bioluminescence of the metastases every 2 days. We observed that oxaliplatin at 8 mg/kg did not show any antitumor effect (Figure 1E), whereas the activity of DACHPt/m at 3 mg/kg against lymph node metastases was significant (Figure 1E) and comparable to that of the micelles in the metastases coexisting with primary tumors (Figure 1D). The visual examination of representative lymph nodes collected 15 days after treatment (Figure 1F) supports the outstanding activity of micelles in this metastatic model. The ability of systemically injected DACHPt/m to treat lymph node metastases after resection of primary tumors suggests that the micelles are likely to reach the metastasis in the lymph nodes *via* the blood vascular route.

DACHPt/m Preferentially Accumulated in Metastatic Lymph Nodes. As the activity of the micelles is associated with their accumulation in malignant tissues, we determined the levels of intravenously injected DACHPt/m as well as free oxaliplatin in whole metastatic lymph nodes, that is, lymph nodes including tumor tissues. Metastatic lymph nodes having metastatic niches of approximately 200 μm and healthy brachial lymph nodes from the opposite flank of mice were collected 24 h after administration of oxaliplatin or DACHPt/m at 5 mg/kg based on DACHPt, and the Pt concentration in these tissues was determined by inductively coupled plasma-mass spectrometry (ICP-MS). The accumulation of oxaliplatin in metastatic lymph nodes, which was approximately 0.04 μg/lymph node, was comparable to that in healthy lymph nodes, showing no selectivity for oxaliplatin to metastatic lymph nodes (Figure 2A). Conversely, the accumulation of micelles in metastatic lymph nodes (0.27 μg/lymph node; approximately 20% of injected dose/g of tissue) was significantly higher than that in healthy lymph nodes, indicating the selectivity of the micelles toward tumor-bearing lymph nodes (Figure 2A). Moreover, the accumulation of DACHPt/m in metastatic lymph nodes did not depend on the presence of primary tumors, as the Pt levels in metastatic lymph nodes coexisting with primary tumors were comparable with those in metastatic lymph nodes after resecting the primary tumor (Figure 2A).
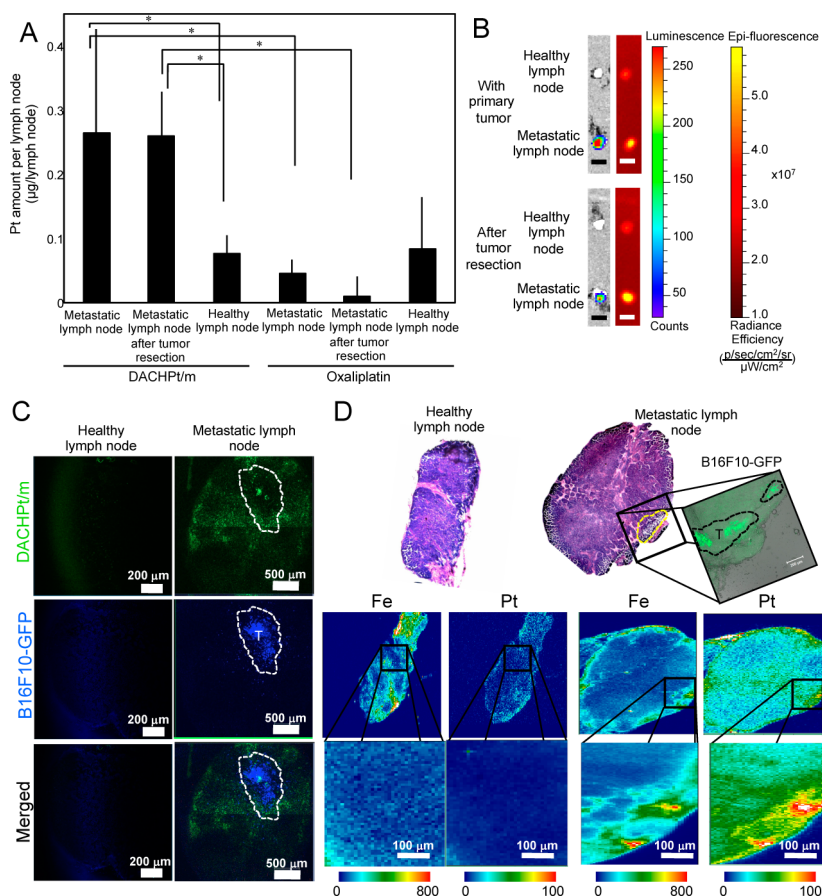
Figure 2. Accumulation of DACHPt-loaded micelles (DACHPt/m) in metastatic lymph nodes. (A) Pt accumulation in metastatic lymph nodes and healthy lymph nodes 24 h after injection of oxaliplatin or DACHPt/m at 5 mg/kg. Data presented as mean ± SD ($n = 6$). *$p < 0.05$ determined by Student's t test. **(B)** *Ex vivo* imaging of healthy lymph nodes and lymph nodes having bioluminescent metastasis of B16-F10-luc cells after the administration of Alexa 647-labeled DACHPt/m. **(C)** Fluorescent microscopies of healthy lymph nodes and metastatic lymph nodes 24 h after injection of Alexa 647-labeled DACHPt/m (green). B16-F10-GFP cells are observed in blue (dotted line). **(D)** Pt and Fe microdistribution by μ-SR-XRF in healthy lymph nodes and metastatic lymph nodes 24 h after injection of DACHPt/m at 20 mg/kg. Fluorescence microscopy indicates the presence of B16-F10-GFP metastasis (green; dotted line).

This enhanced accumulation of micelles in metastatic lymph nodes was also confirmed by systemically injecting DACHPt/m labeled with Alexa 647 (Figure 2B) in mice bearing lymph node metastasis with primary tumors or after tumor resection. The fluorescent signal from these micelles was found to be approximately 4-fold higher in metastatic lymph nodes than in the contralateral healthy lymph nodes, regardless of the presence of the primary tumor. These results support the superior antitumor effect of DACHPt/m against lymph node metastasis.

The microdistribution of intravenously administered micelles in metastatic lymph nodes was studied by fluorescence microscopy of tissue sections. For that, mice were inoculated with melanoma cells expressing GFP (B16-F10-GFP) in the forepaw and allowed to grow until lymph node metastases were formed. Then, the primary tumors were removed, and 24 h later DACHPt/m labeled with Alexa 647 were intravenously injected. Metastatic and healthy lymph nodes were collected 24 h after micelles administration. Thus, while the fluorescence from the micelles was not observed in healthy lymph nodes (Figure 2C), it was clearly detectable within the metastatic lymph nodes (Figure 2C; green), indicating accumulation of micelles within the whole lymph node section. Moreover, the microdistribution of DACHPt delivered by the micelles in metastatic lymph nodes was determined by using μ-synchroton radiation-X-ray fluorescence (μ-SR-XRF), which allows mapping endogenous and exogenous elements present in tissue sections.[37] Thus, the Pt mapping for DACHPt/m showed higher Pt levels within the metastatic lymph nodes than in healthy lymph nodes, where the Pt signal from the micelles was undetectable (Figure 2D). Moreover, the colocalization of Pt from micelles with Fe from hemeproteins of blood within the lymph node metastases suggests that micelles could reach the metastasis through the blood supply. Previous dynamic contrast-enhanced MRI studies using small gadolinium contrast agents and gadolinium-conjugated albumin have demonstrated an increase in the permeability of blood capillaries in metastatic lymph nodes,[38,39] which may

TABLE 2. *In Vitro* Cytotoxicity of Oxaliplatin, Doxil, and DACHPt-Loaded Micelles (DACHPt/m) with 30 and 70 nm Diameter against B16-F10-luc Cells

	IC$_{50}$ (μM)[a]			
time (h)	Oxaliplatin	Doxil[b]	30 nm DACHPt/m[c]	70 nm DACHPt/m[c]
48	5.0 ± 0.2	0.6 ± 0.1	3.5 ± 0.3	8.0 ± 0.2
72	2.6 ± 0.1	0.2 ± 0.1	1.3 ± 0.2	0.4 ± 0.1

[a] Determined by MTT assay (n = 8; mean ± SD). [b] Based on doxorubicin. [c] Based on DACHPt.

facilitate the preferable accumulation of micelles in metastatic lymph nodes over healthy lymph nodes.

Targeting Efficiency of DACHPt/m and Doxil against Lymph Node Metastases. To investigate the mechanisms driving the targeting of DACHPt/m after systemic injection, we compared the targeting efficiency of the micelles with that of clinically approved Doxil, *i.e.*, PEGylated liposomes incorporating doxorubicin, as PEGylated liposomes have shown limited delivery to lymph node metastases after systemic administration.[31,32] The size distribution of these carriers was determined by dynamic light scattering (DLS), showing that the micelles and Doxil have narrowly distributed diameters, which were 30 and 80 nm, respectively (Table 1). The diameters were also confirmed by transmission electron microscopy TEM (Table 1 and Supporting Information Figure S2). It is worth noticing that the diameters of the micelles observed in TEM are slightly smaller than those of DLS, since the PEG shell cannot be observed due to the lower electron density. The surface charge of both carriers was close to neutral due to their dense PEG shells (Table 1).

The *in vitro* activity of both DACHPt/m and Doxil was evaluated by incubating the carriers with B16-F10-Luc cells for 48 and 72 h, showing higher activity for Doxil than for the micelles (Table 2). Conversely, the *in vivo* efficacy of Doxil in lymph node metastasis after resecting the primary tumors was found to be lower than that of micelles. Accordingly, Doxil intravenously injected 3-times every second day at 2 mg/kg on a doxorubin basis failed to suppress the metastatic growth, while at 4 mg/kg, it was toxic (Figure 3A,B), probably due to the prompt administration, which could lead to a high cumulative dosage. In contrast, despite being less effective *in vitro* (Table 2), DACHPt/m at 3 mg/kg inhibited the growth of the metastases in the lymph nodes (Figure 3A), suggesting that their ability to reach metastases in lymph nodes may be more efficient than that of Doxil.

We therefore studied the real-time microdistribution of Doxil and Alexa 647-labeled DACHPt/m in metastatic lymph nodes by using *in vivo* confocal laser scanning microscopy (CLSM). This *in vivo* CLSM technique allows spatiotemporal and quantitative analyses of blood circulation, extravasation and tissue penetration in living animals.[40] To directly observe the metastatic niche in lymph nodes, we inoculated B16-F10-GFP cells in the forepaw of mice, and allowed the primary tumors to grow for 2 weeks. Then, primary tumors were surgically removed, leaving only the lymph node metastases, which were imaged by *in vivo* CLSM 48 h later (Figure 3C, before, dotted line). After fixing the position of the lymph node for continuous observation, both Doxil and Alexa 647-labeled DACHPt/m were co-injected, and the fluorescent signals from doxorubicin in the liposomes and the fluorescent dye in the micelles were simultaneously quantified in the blood vessels, the interstitial space of metastatic lymph nodes and the metastatic site. Both Doxil and Alexa 647-DACHPt/m showed comparable prolonged circulation in the bloodstream (Figure 3C and Supporting Information Movie S1). However, the microdistribution of the nano-carriers in the metastatic lymph nodes was contrasting, showing that even though Doxil was able to extravasate and accumulate in peritumoral regions, it failed to penetrate within the metastatic focus (Figure 3C and Supporting Information Movie S1), whereas DACHPt/m gradually extravasated and penetrated inside the tumor mass (Figure 3C, dotted line and Supporting Information Movie S1). Six-hours after co-injection, the difference between DACHPt/m and Doxil within the metastasis was evident, as DACHPt/m had achieved a deep and broad distribution (Figure 3C, white square). By quantifying the time-lapse fluorescent signal, which was normalized to the maximum fluorescence achieved by the nanocarrier in the blood vessels, we demonstrated that the micelles gradually accumulated in the metastatic region (Figure 3D). In healthy lymph nodes, we observed that DACHPt/m did not extravasate and the fluorescence signal from the micelles was always detectable within the blood vessels (Supporting Information Figure S3 and Supporting Information Movie S2). *In vivo* CLSM results indicate enhanced permeability in metastatic lymph nodes as intravenously injected DACHPt/m can reach the cancer cells in the lymph nodes through the blood vessels in lymph node metastasis, and suggest that the effective extravasation and penetration of the nanocarrier in the metastases was determinant for achieving a strong antitumor activity. Because PEGylated liposomes with comparable diameter to Doxil have been reported to remain in perivascular regions of tumors,[41] supporting our intravital microscopic observations for Doxil penetration in the lymph node metastasis, and we have previously reported that the size of nanocarriers in the sub-100 nm range critically affected their penetration and accumulation in poorly permeable tumors, and their eventual therapeutic efficacy,[33] we hypothesized that this difference in penetration in the metastatic site may be due to the larger size of Doxil (80 nm) than that of DACHPt/m (30 nm). Since Doxil and DACHPt/m have several other differences besides their size, such as surface chemistry, drug
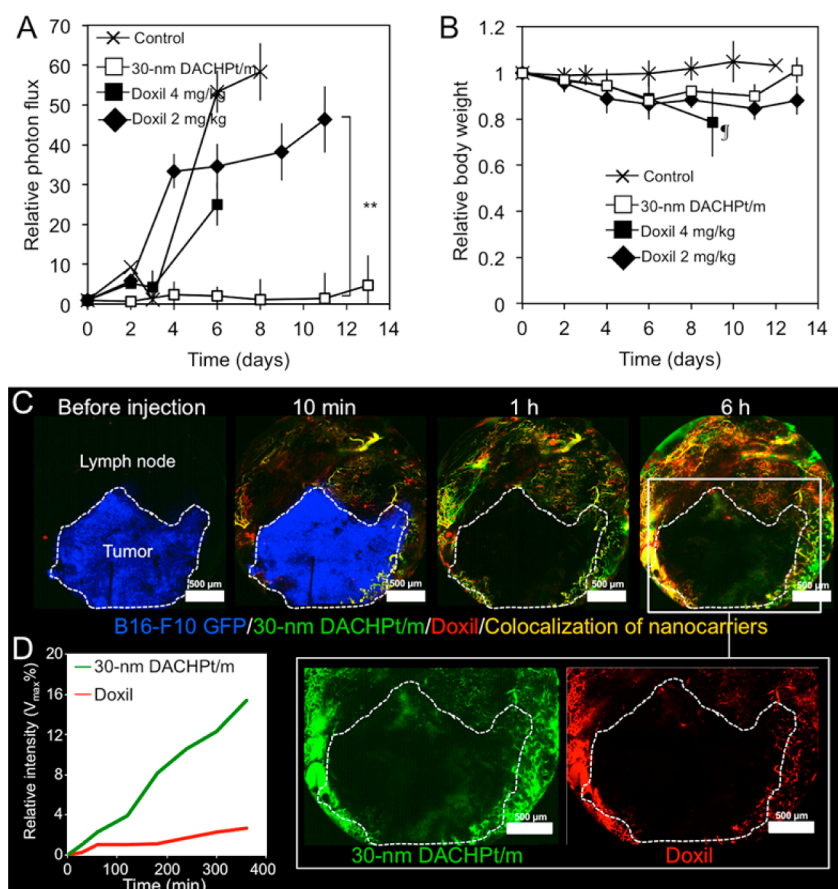
Figure 3. Targeting ability of DACHPt-loaded micelles (DACHPt/m) and Doxil against lymph node metastasis. (A) Relative photon flow from bioluminescent lymph node metastasis in mice treated with DACHPt/m and Doxil. Primary tumors were removed after detection of the metastasis in lymph nodes. Mice received saline, Doxil at 2 and 4 mg/kg, and micelles at 3 mg/kg on days 0, 2, and 4. Data presented as mean $\pm$ SD ($n = 5$). **$p < 0.01$ determined by ANOVA with Tukey's multiple comparison test. (B) Relative body weight of mice during the antitumor activity experiment. Symbo (¶) = 2/5 toxic deaths. (C) Time-lapse intravital microscopies of metastatic lymph nodes before and after co-injection of Alexa 647-labeled DACHPt/m (green) and Doxil (red). B16F10-GFP metastasis are shown as blue (enclosed by dotted line). Signal from B16F10-GFP cells was removed in 1 and 6 h snapshots to facilitate the observation. Magnification of metastatic region at 6 h after injection (white square) and splitted channels for DACHPt/m (green) and Doxil (red) showing the enhanced tumor penetration and accumulation of micelles. (D) Quantification of the changes in the fluorescence signals within the metastatic region (enclosed area by dotted line in panel C).

release, stability and pharmacokinetics, to verify this hypothesis, we proceeded to study the *in vivo* performance of DACHPt/m with size comparable to Doxil.

The Size of DACHPt/m Affected the Targeting Efficiency against Lymph Node Metastasis. Because the size of DACHPt/m can be directly tailored by adding poly-(glutamic acid) (P(Glu)) homopolymer to the reaction mixture of DACHPt and PEG-*b*-P(Glu) copolymer,[33] we tested our above-mentioned hypothesis by comparing the targeting efficiency of DACHPt/m having 30 nm diameter, which are obtained without homopolymer, with that of DACHPt/m with 70 nm diameter, which is comparable to the diameter of Doxil (Table 1 and Supporting Information Figure S2). DACHPt/m with 30 and 70 nm have shown similar stability, zeta potential, drug release rate and plasma clearance,[33] allowing to study the effect of their size on the penetration and accumulation in tumors, and the resulting therapeutic outcome. Moreover, from our previous observations

showing that 70 nm micelles are retained in perivascular regions of hypopermeable tumors even after 24 h,[33] it can be inferred that the break down of the micelles into unimers does not influence their dissemination in tumors, and that the differences in tumor penetration of the micelles are mainly based on their diameters.

We initially confirmed that the *in vitro* activity of 30 and 70 nm micelles against B16-F10-Luc cells was comparable (Table 2; $p > 0.05$). The *in vivo* activity of 30 and 70 nm micelles was then evaluated against lymph node metastasis after resecting the primary tumors. We observed that both 30 and 70 nm DACHPt/m at 3 mg/kg on a DACHPt basis restricted the growth of the metastasis, with 30 nm DACHPt/m being more potent than 70 nm DACHPt/m (Figure 4A). These data support our hypothesis that the size of nanocarriers affects their activity against the metastasis in the lymph nodes, associated with the ability to reach these metastases.
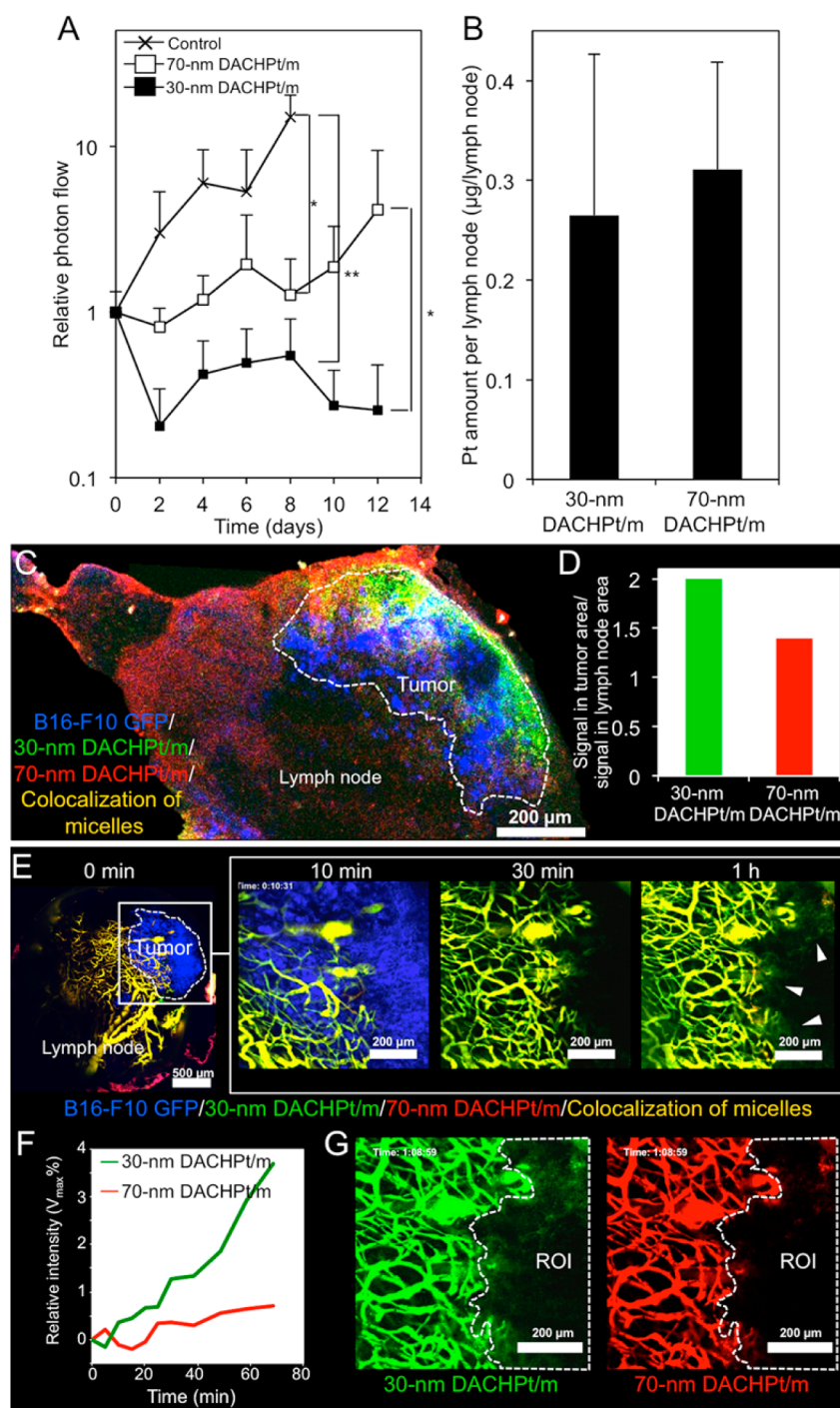
Figure 4. Effect of the size of DACHPt-loaded micelles (DACHPt/m) on their targeting against lymph nodes metastasis. (A) Relative photon flow from bioluminescent lymph node metastasis in mice treated with 30 and 70 nm DACHPt/m after resection of primary tumors. Mice received saline, and micelles at 3 mg/kg on days 0, 2, and 4. Data are mean ± SD ($n = 5$). *$p < 0.05$; **$p < 0.01$ determined by ANOVA with Tukey's multiple comparison test. (B) Pt accumulation of 30 and 70 nm DACHPt/m in metastatic lymph nodes 24 h after injection. Data are mean ± SD ($n = 6$). (C) Fluorescence microscopy of metastatic lymph node 24 h after co-injection of fluorescent-labeled 30 (green) and 70 nm (red) DACHPt/m. B16F10-GFP metastasis appears in blue and micelles colocalization in yellow. (D) Ratio of the fluorescence intensity of micelles in the metastatic region *versus* their intensity in lymph node region. (E) Time-lapse intravital microscopies of metastatic lymph nodes after co-injection of fluorescent-labeled 30 (green) and 70 nm (red) DACHPt/m. To facilitate observation, tumor region was magnified (white square) and the tumor signal was removed in 30 min and 1 h snapshots. White arrowheads indicate extravasation for 30 nm DACHPt/m. (F) Changes in fluorescent signals for 30 (green) and 70 nm DACHPt/m (red) in the metastatic region marked with dotted line (G).

The accumulation of DACHPt/m with 30 or 70 nm diameter was studied in whole metastatic lymph nodes, that is, lymph nodes including tumor tissues, 24 h after intravenous injection. Both 30 and 70 nm

micelles showed comparable high Pt levels in metastatic lymph nodes (Figure 4B), suggesting that the difference in the activity of the micelles may be related to their microdistribution in the nodes. Thus, the microdistribution of the micelles in lymph nodes having B16-F10-GFP metastasis was studied by co-injecting 30 nm DACHPt/m labeled with Alexa 647 and 70 nm DACHPt/m labeled with Alexa 555. It is worth noting that the conjugation of fluorescent probes to the 30 and 70 nm micelles did not affect their stability in physiological conditions, and both micelles were demonstrated to maintain their original size for more than 48 h (Supporting Information Figure S4), which is suitable for studying their microdistribution in relevant time periods. Thus, 24 h after micelles' administration, the metastatic lymph nodes were collected, and tissue sections were studied by fluorescence microscopy (Figure 4C). The micelles with 30 nm diameter (Figure 4C; green) showed 2-fold higher fluorescent signal in the metastatic region (Figure 4C; blue) than in the lymph node (Figure 4D), while the intensity of 70 nm micelles (Figure 4C; red) in the metastatic focus was only 1.4-fold greater than that in the lymph node (Figure 4D). The results were further validated by exchanging the fluorescent labels of the micelles, *i.e.*, 30 nm micelles were marked with Alexa 555 and 70 nm micelles were labeled with Alexa 647, and studying their microdistribution in metastatic lymph nodes. Again, the 30 nm micelles showed higher accumulation in the metastatic focus than 70 nm micelles (Supporting Information Figure S5), supporting the higher selectivity for 30 nm micelles than for 70 nm micelles for the metastasis in lymph nodes, which may be associated with the ability of the micelles for reaching the metastatic region.

To compare the dynamic processes of extravasation and penetration of the micelles in the metastatic lymph nodes, their real-time microdistribution in metastatic lymph nodes having B16-F10-GFP metastasis was studied by *in vivo* CLSM. Alexa 555-labeled DACHPt/m with 30 nm diameter and Alexa 647-labeled DACHPt/m with 70 nm diameter were co-injected and their fluorescent signals in the blood vessels and metastatic lymph nodes were concurrently evaluated. The fluorescent intensity of both micelles in the blood vessels was comparable, corroborating their prolonged life in the bloodstream (Figure 4E and Supporting Information Movie S3).[33−35] However, the extravasation and penetration of 30 nm DACHPt/m in the metastasis occurred more rapidly than for 70 nm DACHPt/m (white arrowheads in Figure 4E and Supporting Information Movie S3). By quantifying the time-lapse fluorescent signals within the tumor mass (area encircled by dotted line in Figure 4G), which were normalized to the maximum fluorescence achieved by the micelles in the blood vessels, we observed that 30 nm DACHPt/m gradually accumulated in the metastatic region (Figure 4F), whereas the accumulation of the 70 nm DACHPt/m was limited. Similar results were observed for smaller lymphatic metastasis, suggesting that the size-restricted penetration and accumulation is also present during former stages (Supporting Information Figure S6). Moreover, our intravital microscopies demonstrated lower permeability in the cluster of cancer cells than in the surrounding lymph node tissue, as only 30 nm DACHPt/m were capable to penetrate within the metastases, whereas larger nanocarriers mainly extravasated in the periphery of the metastatic foci. Thus, this size-dependent permeability of the metastases in lymph nodes, and the extended life of micelles in the bloodstream, which allows supply of drugs to the cancer cells for prolonged time, promoted the superior efficacy of 30 nm DACHPt/m.

CONCLUSION

Our results demonstrated the ability of systemically injected DACHPt/m for targeting lymph node metastasis through the blood vascular route, highlighting the importance of the size of the nanocarriers for reaching the metastatic foci, as larger nanocarriers, *i.e.*, Doxil and 70 nm DACHPt/m, failed to penetrate within the metastatic site. This selective accumulation in metastatic lymph nodes and their resilient therapeutic effect indicate the potential of polymeric micelles as nanocarriers for noninvasive management of nodal disease. The possibility to target lymph node metastasis by systemically administered nanocarriers offers enormous advantages over locally injected agents, as invasive local procedures and multiple injections in one setting are substituted by an intravenous injection, while any lymph node involved in the metastatic setting may be plausible for targeting, regardless of the anatomical position. Such conservative treatments have the potential for reducing the risk of relapse, while enhancing survival and quality of life of patients.

METHODS

Materials. *N,N*-Dimethylformamide (DMF) and 3-(4,5-dimethylthiazol-2-yl)-2,5-diphenyltetrazolium bromide (MTT) were purchased from Wako Pure Chemicals Industries, Ltd. (Tokyo, Japan). Dichloro(1,2-diammino cyclohexane) platinum(II) was purchased from W.C. Heraeus GmbH (Hanau, Germany). γ-Benzyl L-glutamate, oxaliplatin, and RPMI 1640-cell culture medium were obtained from Sigma-Aldrich Co., Inc. (St. Louis, MO). Bis(trichloromethyl) carbonate (triphosgene) was purchased from Tokyo Kasei Kogyo, Co. Ltd. (Tokyo, Japan). α-Methoxy-ω-amino-poly(ethylene glycol) (CH₃O-PEG-NH₂; MW, 12 000) was bought from NOF Co., Ltd. (Tokyo, Japan). Doxil was purchased from Alza Corporation (Vacaville, CA). Luciferin was acquired from Promega (Madison, WI).

Cell Lines and Animals. Murine melanoma B16-F10 cells expressing luciferase (B16-F10-luc) were purchased from Caliper LifeSciences (Hopkinton, MA). B16-F10 cells expressing GFP were purchased from Anticancer, Co. (San Diego, CA). Cells were maintained in RPMI 1640 medium containing 10% fetal bovine serum (FBS) in a humidified atmosphere containing 5% CO_2 at 37 °C. Immunocompetent C57BL6-J mice (female; 18−20 g body weight; age, 6 weeks) were purchased from Charles River Japan (Kanagawa, Japan). All animal experiments were performed in accordance with the Guidelines for the Care and Use of Laboratory Animals as stated by The University of Tokyo.

Synthesis of Polymers. Poly(ethylene glycol)-b-poly(L-glutamic acid) [PEG-b-P(Glu)] copolymer [Molecular weight of PEG (MW$_{PEG}$, 12 000; polymerization degree of P(Glu), 40] and poly(L-glutamic acid) [P(Glu), polymerization degree of P(Glu), 40] were synthesized according to the previously described method.[33] N-Carboxyanhydride of γ-benzyl L-glutamate (BLG-NCA) was polymerized in DMF initiated by the amino group of CH_3O-PEG-NH_2, or in DMSO initiated by n-butylamine, to obtain PEG-b-poly(γ-benzyl L-glutamate) (PEG-b-PBLG) copolymer or poly(γ-benzyl L-glutamate) (PBLG) homopolymer, respectively. The MW distributions of PEG-b-PBLG and PBLG were determined to be approximately 1.16 and 1.2, respectively, by gel permeation chromatography (GPC) [column, TSK-gel G3000HHR, G4000HHR (Tosoh)]. The degree of polymerization of PBLG in both PEG-b-PBLG and PBLG was confirmed to be 40 by comparing the proton ratios of methylene units in PEG ($-OCH_2CH_2-$: $d = 3.7$ ppm) for the block copolymer, or the butyl group for the homopolymer, with the phenyl groups of PBLG ($-CH_2C_6H_5$: $d = 7.3$ ppm) in ^1H NMR spectra [JEOL EX270 (JEOL Inc., Tokyo, Japan); temperature, 70 °C; solvent, DMSO-d_6]. The degree of polymerization of PBLG homopolymer was verified to be 40 by comparing the proton ratios of the methylene units in in the butyl end ($-CH2$-: $\delta = 1.35$ ppm and $\delta = 1.55$ ppm) with the phenyl groups of PBLG by ^1H NMR. Polymers were deprotected by mixing with 0.5 N NaOH at room temperature to obtain PEG-b-P(Glu) copolymer and P(Glu) homopolymer. Complete deprotection was confirmed by ^1H NMR. For the preparation of fluorescent labeled PEG-b-P(Glu), Alexa 647-NHS or Alexa 555-NHS was mixed with the copolymer in DMSO, dialyzed against water and purified by column filtration. The labeling of Alexa 647 or Alexa 555 on PEG-b-P(Glu) polymers was 10% mol/mol.

Preparation Of DACHPt-Loaded Polymeric Micelles (DACHPt/m). DACHPt-loaded polymeric micelles (DACHPt/m) were prepared according to the previously described method.[33,34] Dicholoro salt of DACHPt (5 mM) was suspended in distilled water and mixed with silver nitrate ($[AgNO_3]/[DACHPt] = 1$) to form DACHPt nitrate chloride at 25 °C for 24 h. The resulting AgCl precipitates were removed by centrifugation. The supernatant was further purified by passage through a 0.22-μm filter. DACHPt nitrate chloride solution was then mixed with PEG-b-P(Glu) copolymer ([Glu] = 5 mM; [DACHPt]/[Glu] = 1.0) and reacted for 120 h to obtain DACHPt/m. For preparing 70 nm micelles, 0.5 mM P(Glu) homopolymer was added to the reaction mixture of DACHPt nitrate chloride and PEG-b-P(Glu) copolymer. Micelles were purified by ultrafiltration (MWCO, 30 000 Da). Moreover, Alexa 647- and Alexa 555-labeled DACHPt/m with 30 and 70 nm diameters were prepared by using PEG-b-P(Glu)-Alexa 647 and PEG-b-P(Glu)-Alexa 555, respectively. The platinum content of all micelles was determined by ion-coupled plasma mass spectrometry (4500 ICP-MS; Hewlett-Packard). Moreover, the stability of Alexa 647-labeled DACHPt/m with 30 nm diameter and Alexa 555-labeled micelles with 70 nm diameter was evaluated in physiological conditions. Accordingly, the micelles were diluted at a final concentration of 0.5 mg/mL in 10 mM PBS plus 150 mM NaCl, and the size was evaluated by dynamic light scattering at defined time points, with Alexa 647-labeled micelles being studied with a Zetasizer having a 532 nm laser and Alexa 555-labeled micelles with a Zetasizer equipped with the standard 633 nm laser.

In Vitro Cytotoxicity. The in vitro cytotoxicity of oxaliplatin, Doxil, and DACHPt/m with 30 and 70 nm diameters was examined against B16-F10-luc. Cancer cells were plated into flat-bottomed 96-well plates at 2.5×10^3 cells per well, and treated by continuous exposure to different concentrations of oxaliplatin, Doxil or DACHPt/m in a final volume of 100 μL. Plates were incubated for 48 h at 37 °C in a humidified atmosphere with 5% CO_2, and cell viability was determined by MTT assay. The significance of the results was analyzed by Student's t test.

Preparation of Tumor Models. C57BL6-J mice were inoculated in the left forepaw with B16-F10-luc cells (1×10^8 cells/mL; 10 μL/mouse) to prepare a syngeneic melanoma model. These tumors spontaneously formed lymph node metastasis in the brachial lymph nodes. For evaluating the bioluminescence from lymph node metastasis, the left flank of mice having primary B16-F10-luc tumors in the forepaw was shaved for easy detection of the bioluminescence of the lymph node metastasis. In vivo imaging of the luciferase activity in the brachial lymph nodes was followed by using an IVIS imaging system (Caliper Life Sciences Co., Inc. (Hopkinton, MA)). Mice were anesthetized with isoflurane and injected intraperitoneally with 150 mg/kg of luciferin. The animals were imaged 10 min after luciferin injection. To minimize the variability of the bioluminescent signal during the antitumor activity experiment, the formation of metastasis was followed daily. As soon as the metastases in the lymph nodes were discovered, mice were divided in two groups, i.e., mice having primary tumors and lymph node metastasis and mice having lymph node metastasis but with their primary tumors resected. For preparing the latter group, the whole B16-F10-luc tumor in the forepaw of mice was surgically removed, mice were sutured, and the luciferase signal was confirmed to be solely at the lymph nodes. The evaluation of the antitumor activity of the drugs was initiated 24 h after the metastases were detected. This procedure allowed us to have metastasis with initial bioluminescent intensity, facilitating the evaluation of the antitumor effects of drugs and reducing the deviation throughout the antitumor activity experiment. For preparing fluorescent lymph node metastasis, B16-F10-GFP cells (1×10^8 cells/mL; 10 μL/mouse) were inoculated in the left forepaw of C57BL6-J mice.

Histology of Lymph Node Metastasis. After detection on the metastasis, the metastatic lymph node of mice were collected and fixed in 4% paraformaldehyde. For H&E staining, the metastatic lymph nodes were embedded in paraffin to prepare the tissue sections. Samples were observed under an AX80 microscope (Olympus, Tokyo, Japan).

In Vivo Antitumor Activity against Primary Tumors. B16-F10-luc tumors in the forepaw of mice were allowed to grow for 4 days (the size of tumor at this point was approximately 3 mm³). Then, mice were randomized in groups (n = 5) and the anticancer effect of the drugs against primary tumors was evaluated by intravenously injecting in the tail vein oxaliplatin at 8 mg/kg and DACHPt/m with 30 nm at 3 mg/kg on a DACHPt basis, 3 times at 2-day intervals. The antitumor activity was evaluated in terms of tumor size (V) estimated by the following equation:

$$V = a \times b^2/2$$

where a and b are the major and minor axes of the tumor, respectively, as measured by a caliper. The statistical significance between the groups was determined by ANOVA with Tukey's multiple comparison test. The results were considered statistically significant if two-tailed P-values were lower than 0.05.

In Vivo Antitumor Activity against Lymph Node Metastasis. Mice having both primary tumors and lymph node metastasis (n = 5) as well as mice having lymph node metastasis but with their primary tumors resected (n = 5) were intravenously injected in the tail vein with oxaliplatin at 8 mg/kg, Doxil at 2 and 4 mg/kg on a doxorubicin basis, and 30 and 70 nm DACHPt/m at 3 mg/kg on a DACHPt basis 3 times at 2-day intervals. The bioluminescence signal from the lymph node metastasis was followed every 2 days. For that, mice were anesthetized with isoflurane and injected intraperitoneally with 150 mg/kg of luciferin. The animals were imaged 10 min after luciferin injection. The bioluminescent signal was quantified in the region of interest by using the in vivo imaging software (Caliper Life Sciences Co., Inc.). The statistical significance between the groups was determined by ANOVA with Tukey's multiple comparison test.

The results were considered statistically significant if two-tailed *P*-values were lower than 0.05.

Accumulation of Drugs in Metastatic Lymph Nodes. The accumulation of oxaliplatin and DACHPt/m with 30 and 70 nm diameter in brachial metastatic lymph nodes and contralateral healthy lymph nodes was determined by using mice having primary tumor and lymph node metastasis, as well as mice having lymph node metastasis but with their primary tumors resected. The metastatic lymph nodes and healthy brachial lymph nodes from the right flank were excised 24 h after administration of the drugs. The samples were weighed, dissolved in hot HNO_3 and evaporated to dryness. Then, 1 mL of 1% HCl solution was added and the Pt concentrations were measured by ICP-MS. Statistical analysis was performed by Student's *t* test. The accumulation of the micelles in metastatic lymph nodes was also assessed through *in vivo* fluorescence imaging by using Alexa 647-labeled DACHPt/m. Fluorescent micelles were intravenously injected to mice having primary tumor and lymph node metastasis, as well as to mice having lymph node metastasis and their primary tumors resected. Twenty-four hours later, metastatic lymph nodes and healthy brachial lymph nodes from the right flank were excised and the bioluminescence was imaged to demonstrate their metastatic condition. The fluorescence Alexa 647-labeled DACHPt/m in the tissues was imaged by IVIS using an excitation filter of 640 nm and an emission filter of 680 nm.

***In Vivo* Confocal Laser Scanning Microscopy.** The *in vivo* confocal laser scanning microscopy (CLSM) observation was performed according to the previously reported method,[40] which was adapted for imaging the metastatic lymph nodes in real time. Accordingly, 48 h after resecting the primary tumor, the brachial lymph node of mice bearing B16-F10-GFP lymph node metastasis was surgically exposed and the lymph node position was fixed by using a vacuum system as previously reported.[42] Then, Doxil at a dose of 20 mg/kg and Alexa 647-labeled 30 nm DACHPt/m at a dose of 10 mg/kg on a DACHPt basis, or Alexa 647-labeled 30 nm DACHPt/m and Alexa 555-labeled 70 nm DACHPt/m both at a dose of 10 mg/kg on a DACHPt were intravenously co-injected in the tail vein. All *in vivo* picture acquisitions were performed using a Nikon A1R confocal laser scanning microscope system attached to an upright ECLIPSE FN1 (Nikon, Japan). Doxorubicin in Doxil was detected using 488/520 nm excitation/emission filters, while the signal from Alexa 555-labeled micelles was followed by using 560/620 nm excitation/emission filters and the signal from Alexa 647-labeled micelles was acquired with 633/670 excitation/emission filters. The real-time microdistribution of Alexa 647-labeled micelles was also observed in healthy lymph nodes.

Fluorescence Microscopy of Metastatic Lymph Nodes. The microdistribution of fluorescent micelles in the lymph nodes was also studied in tissue sections. Thus, Alexa 647-labeled DACHPt/m having 30 nm diameter (10 mg/kg on DACHPt basis) and Alexa 555-labeled DACHPt/m having 70 nm diameter (10 mg/kg on DACHPt basis) were intravenously co-injected to mice bearing lymph nodes metastasis of B16-F10-GFP having their primary tumors resected. The metastatic lymph nodes were collected 24 h after injection, embedded in optimal cutting temperature (OCT) compound and frozen in an ethanol/liquid N_2 mixture. Frozen samples were sectioned at 6 μm thickness in a cryostat, and fixed in acetone. The samples were observed by using a Zeiss LSM780 confocal microscope (Oberkochen, Germany).

Element Microdistribution in Lymph Nodes Using μ-X-ray Fluorescence. Synchrotron radiation-induced X-ray fluorescence spectrometry imaging (SR-XRF) was used to determine the distribution of DACHPt and Fe in sections of healthy lymph nodes and lymph nodes having B16-F10-GFP metastasis at 24 h postintravenous injection of 30 nm DACHPt/m. Briefly, C57BL6-J mice having lymph node metastasis of B16-F10-GFP cells were intravenously injected in the tail vein with 30 nm DACHPt/m and 70 nm DACHPt/m at 20 mg/kg on a DACHPt basis. Twenty-four hours later, healthy lymph nodes and metastatic lymph nodes were collected, embedded in OCT compound, immediately frozen in an ethanol/liquid N_2 mixture, and then sliced at 20 μm thickness using a cryostat and fixed on polypropylene sheets. μ-SR-XRF was performed using beamline 37XU at SPring-8 (Hyogo, Japan),

operated at 8 GeV and ~100 mA. A photon beam with 14 keV of energy, a beam spot size of 1.3 $\times$ 1.3 μm^2, and an intensity of 1 $\times$ 10^{12} photons/s was used to irradiate the tissue sample. Each sample was mounted on an *x*−*y* translation stage and the fluorescence X-rays were measured using a Si-SSD in air at room temperature. The fluorescence X-ray intensity was normalized by the incident X-ray intensity, I_0, to produce a two-dimensional elemental map.

Conflict of Interest: The authors declare no competing financial interest.

Supporting Information Available: Supporting Information including the preparation of the metastatic model, the TEM evaluation of the nanocarriers, the time-lapse *in vivo* microscopy of the behavior of micelles in healthy lymph nodes, the time-lapse *in vivo* microscopy of the accumulation of micelles in micrometastasis, and Supporting Information movies of the real-time microdistribution of the nanocarriers in lymph nodes. This material is available free of charge *via* the Internet at http://pubs.acs.org.

REFERENCES AND NOTES

1. Hess, K. R.; Varadhachary, G. R.; Taylor, S. H.; Wei, W.; Raber, M. N.; Lenzi, R.; Abbruzzese, J. L. Metastatic Patterns in Adenocarcinoma. *Cancer* **2006**, *106*, 1624–1633.
2. Kawada, K.; Taketo, M. M. Significance and Mechanism of Lymph Node Metastasis in Cancer Progression. *Cancer Res.* **2011**, *71*, 1214–1218.
3. Wada, N.; Duh, Q. Y.; Sugino, K.; Iwasaki, H.; Kameyama, K.; Mimura, T.; Ito, K.; Takami, H.; Takanashi, Y. Lymph Node Metastasis From 259 Papillary Thyroid Microcarcinomas: Frequency, Pattern of Occurrence and Recurrence, and Optimal Strategy for Neck Dissection. *Ann. Surg.* **2003**, *237*, 399–407.
4. van Dongen, J. A.; Voogd, A. C.; Fentiman, I. S.; Legrand, C.; Sylvester, R. J.; Tong, D.; van der Schueren, E.; Helle, P. A.; van Zijl, K.; Bartelink, H. Long-Term Results of a Randomized Trial Comparing Breast-Conserving Therapy with Mastectomy: European Organization for Research and Treatment of Cancer 10801 Trial. *J. Natl. Cancer Inst.* **2000**, *92*, 1143–1150.
5. Betticher, D. C.; Hsu Schmitz, S.-F.; Tötsch, M.; Hansen, E.; Joss, C.; von Briel, C.; Schmid, R. A.; Pless, M.; Habicht, J.; Roth, A. D.; et al. Mediastinal Lymph Node Clearance After Docetaxel-Cisplatin Neoadjuvant Chemotherapy is Prognostic of Survival in Patients with Stage IIIA pN2 Non−Small-Cell Lung Cancer: A Multicenter Phase II Trial. *J. Clin. Oncol.* **2003**, *21*, 1752–1759.
6. Alvarado, R.; Yi, M.; Le-Petross, H.; Gilcrease, M.; Mittendorf, E. A.; Bedrosian, I.; Hwang, R. F.; Caudle, A. S.; Babiera, G. V.; Akins, J. S.; et al. The Role for Sentinel Lymph Node Dissection after Neoadjuvant Chemotherapy in Patients Who Present with Node-Positive Breast Cancer. *Ann. Surg. Oncol.* **2012**, *19*, 3177–3184.
7. Minchinton, A. I.; Tannock, I. F. Drug Penetration in Solid Tumors. *Nat. Rev. Cancer* **2006**, *6*, 583–592.
8. Peer, D.; Karp, J. M.; Hong, S.; Farokhzad, O. C.; Margalit, R.; Langer, R. Nanocarriers as an Emerging Platform for Cancer Therapy. *Nat. Nanotechnol.* **2007**, *2*, 751–760.
9. Mura, S.; Nicolas, J.; Couvreur, P. Stimuli-Responsive Nanocarriers for Drug Delivery. *Nat. Mater.* **2013**, *12*, 991–1003.

10. Kataoka, K.; Harada, A.; Nagasaki, Y. Block Copolymer Micelles for Drug Delivery: Design, Characterization and Biological Significance. *Adv. Drug Delivery Rev.* **2001**, *47*, 113–131.

11. Harisinghani, M. G.; Barentsz, J.; Hahn, P. F.; Deserno, W. M.; Tabatabaei, S.; van de Kaa, C. H.; de la Rosette, J.; Weissleder, R. Noninvasive Detection of Clinically Occult Lymph-Node Metastases in Prostate Cancer. *New Eng. J. Med.* **2003**, *348*, 2491–2499.

12. Tseng, Y. C.; Xu, Z.; Guley, K.; Yuan, H.; Huang, L. Lipid−Calcium Phosphate Nanoparticles for Delivery to the Lymphatic System and SPECT/CT Imaging of Lymph Node Metastases. *Biomaterials* **2014**, *35*, 4688–4698.

13. Matsumura, Y.; Maeda, H. A New Concept for Macromolecular Therapeutics in Cancer Chemotherapy: Mechanism of Tumoritropic Accumulation of Proteins and the Antitumor Agent Smancs. *Cancer Res.* **1986**, *46*, 6387–6392.

14. Schroeder, A.; Heller, D. A.; Winslow, M. M.; Dahlman, J. E.; Pratt, G. W.; Langer, R.; Jacks, T.; Anderson, D. G. Treating Metastatic Cancer with Nanotechnology. *Nat. Rev. Cancer* **2012**, *12*, 39–50.

15. Oussoren, C.; Storm, G. Liposomes To Target the Lymphatics by Subcutaneous Administration. *Adv. Drug Delivery Rev.* **2001**, *50*, 143–56.

16. Reddy, S. T.; van der Vlies, A. J.; Simeoni, E.; Angeli, V.; Randolph, G. J.; O'Neil, C. P.; Lee, L. K.; Swartz, M. A.; Hubbell, J. A. Exploiting Lymphatic Transport and Complement Activation in Nanoparticle Vaccines. *Nat. Biotechnol.* **2007**, *25*, 1159–1164.

17. Ryan, G. M.; Kaminskas, L. M.; Porter, C. J. H. Nano-Chemotherapeutics: Maximising Lymphatic Drug Exposure to Improve the Treatment of Lymph-Metastatic Cancers. *J. Controlled Release* **2014**, *193*, 241–256.

18. Thorek, D. L. J.; Ulmert, D.; Diop, N-F. M.; Lupu, M. E.; Doran, M. G.; Huang, R.; Abou, D. S.; Larson, S. M.; Grimm, J. Non-Invasive Mapping of Deep-Tissue Lymph Nodes in Live Animals using a Multimodal PET/MRI Nanoparticle. *Nat. Commun.* **2014**, *5*, Article number: No. 3097.

19. Leong, S. P.; Morita, E. T.; Südmeyer, M.; Chang, J.; Shen, D.; Achtem, T. A.; Allen, R. E., Jr; Kashani-Sabet, M. Heterogeneous Patterns of Lymphatic Drainage to Sentinel Lymph Nodes by Primary Melanoma from Different Anatomic Sites. *Clin. Nucl. Med.* **2005**, *30*, 150–158.

20. Porter, G. A.; Ross, M. I.; Berman, R. S.; Lee, J. E.; Mansfield, P. F.; Gershenwald, J. E. Significance of Multiple Nodal Basin Drainage in Truncal Melanoma Patients Undergoing Sentinel Lymph Node Biopsy. *Ann. Surg. Oncol.* **2000**, *7*, 256–261.

21. Cormier, J. N.; Xing, Y.; Feng, L.; Huang, X.; Davidson, L.; Gershenwald, J. E.; Lee, J. E.; Mansfield, P. F.; Ross, M. I. Metastatic Melanoma to Lymph Nodes in Patients with Unknown Primary Sites. *Cancer* **2006**, *106*, 2012–2020.

22. Perre, C. I.; Hoefnagel, C. A.; Kroon, B. B. R.; Zoetmulder, F. A.; Rutgers, E. J. Altered Lymphatic Drainage after Lymphadenectomy or Radiotherapy of the Axilla in Patients with Breast Cancer. *Br. J. Surg.* **1996**, *83*, 1258.

23. Golse, N.; Lebeau, R.; Lombard-Bohas, C.; Hervieu, V.; Ponchon, T.; Adham, M. Lymph Node Involvement beyond Peripancreatic Region in Pancreatic Head Cancers: When Results Belie Expectations. *Pancreas* **2013**, *42*, 239–248.

24. Nishiyama, N.; Kataoka, K. Current State, Achievements, and Future Prospects ff Polymeric Micelles as Nanocarriers for Drug and Gene Delivery. *Pharmacol. Ther.* **2006**, *112*, 630–648.

25. Cabral, H.; Kataoka, K. Progress of Drug-Loaded Polymeric Micelles into Clinical Studies. *J. Controlled Release* **2014**, *190*, 465–476.

26. Hamaguchi, T.; Kato, K.; Yasui, H.; Morizane, C.; Ikeda, M.; Ueno, H.; Muro, K.; Yamada, Y.; Okusaka, T.; Shirao, K.; et al. A Phase I and Pharmacokinetic Study of NK105, a Paclitaxel-Incorporating Micellar Nanoparticle Formulation. *Br. J. Cancer* **2007**, *97*, 170–176.

27. Hamaguchi, T.; Doi, T.; Eguchi-Nakajima, T.; Kato, K.; Yamada, Y.; Shimada, Y.; Fuse, N.; Ohtsu, A.; Matsumoto, S.; Takanashi, M.; et al. Phase I Study Of NK012, A Novel SN-38−Incorporating Micellar Nanoparticle, in Adult Patients with Solid Tumors. *Clin. Cancer Res.* **2010**, *16*, 5058–5066.

28. Plummer, R.; Wilson, R. H.; Calvert, H.; Boddy, A. V.; Griffin, M.; Sludden, J.; Tilby, M. J.; Eatock, M.; Pearson, D. G.; Ottley, C. J.; et al. A Phase I Clinical Study of Cisplatin-Incorporated Polymeric Micelles (NC-6004) in Patients with Solid Tumors. *Br. J. Cancer* **2011**, *104*, 593–598.

29. Rafi, Md.; Cabral, H.; Kano, M. R.; Mi, P.; Iwata, C.; Yashiro, M.; Hirakawa, K.; Miyazono, K.; Nishiyama, N.; Kataoka, K. Polymeric Micelles Incorporating (1,2-Diaminocyclohexane)-Platinum(II) Suppress the Growth of Orthotopic Scirrhous Gastric Tumors and Their Lymph Node Metastasis. *J. Controlled Release* **2012**, *159*, 189–196.

30. Gershenwald, J. E.; Thompson, W.; Mansfield, P. F.; Lee, J. E.; Colome, M. I.; Tseng, C. H.; Lee, J. J.; Balch, C. M.; Reintgen, D. S.; Ross, M. I. Multi-Institutional Melanoma Lymphatic Mapping Experience: The Prognostic Value of Sentinel Lymph Node Status in 612 Stage I or II Melanoma Patients. *J. Clin. Oncol.* **1999**, *17*, 976–983.

31. Allen, T. M.; Hansen, C. B.; Guo, L. S. Subcutaneous Administration of Liposomes: A Comparison with the Intravenous and Intraperitoneal Routes of Injection. *Biochim. Biophys. Acta* **1993**, *1150*, 9–16.

32. Chen, J. H.; Ling, R.; Yao, Q.; Li, Y.; Chen, T.; Wang, Z.; Li, K. Z. Effect of Small-Size Liposomal Adriamycin Administered by Various Routes on a Metastatic Breast Cancer Model. *Endocr. Relat. Cancer* **2005**, *12*, 93–100.

33. Cabral, H.; Matsumoto, Y.; Mizuno, K.; Chen, Q.; Murakami, M.; Kimura, M.; Terada, Y.; Kano, M. R.; Miyazono, K.; Uesaka, M.; et al. Accumulation of Sub-100 nm Polymeric Micelles in Poorly Permeable Tumors Depends on Size. *Nat. Nanotechnol.* **2011**, *6*, 815–823.

34. Cabral, H.; Nishiyama, N.; Okazaki, S.; Koyama, H.; Kataoka, K. Preparation and Biological Properties of Dichloro(1,2-Diaminocyclohexane)Platinum(II) (DACHPt)-Loaded Polymeric Micelles. *J. Controlled Release* **2005**, *101*, 223–232.

35. Murakami, M.; Cabral, H.; Matsumoto, Y.; Wu, S.; Kano, M. R.; Yamori, T.; Nishiyama, N.; Kataoka, K. Improving Drug Potency and Efficacy by Nanocarrier-Mediated Subcellular Targeting. *Sci. Transl. Med.* **2011**, *3*, 64ra2.

36. Cabral, H.; Murakami, M.; Hojo, H.; Terada, Y.; Kano, M. R.; Chung, U-i.; Nishiyama, N.; Kataoka, K. Targeted Therapy of Spontaneous Murine Pancreatic Tumors by Polymeric Micelles Prolongs Survival and Prevents Peritoneal Metastasis. *Proc. Natl. Acad. Sci. U.S.A.* **2013**, *110*, 11397–11402.

37. Geraki, K.; Farquharson, M. J.; Bradley, D. A. Concentrations of Fe, Cu and Zn in Breast Tissue: A Synchrotron XRF Study. *Phys. Med. Biol.* **2002**, *7*, 2327–2339.

38. Dafni, H.; Cohen, B.; Ziv, K.; Israely, T.; Goldshmidt, O.; Nevo, N.; Harmelin, A.; Vlodavsky, I.; Neeman, M. The Role of Heparanase in Lymph Node Metastatic Dissemination: Dynamic Contrast-Enhanced MRI of Eb Lymphoma in Mice. *Neoplasia* **2005**, *7*, 224–233.

39. Fischbein, N. J.; Noworolski, S. M.; Henry, R. G.; Kaplan, M. J.; Dillon, W. P.; Nelson, S. J. Assessment of Metastatic Cervical Adenopathy Using Dynamic Contrast-Enhanced MR Imaging. *AJNR Am. J. Neuroradiol.* **2003**, *24*, 301–311.

40. Matsumoto, Y.; Nomoto, T.; Cabral, H.; Matsumoto, Y.; Watanabe, S.; Christie, R. J.; Miyata, K.; Oba, M.; Ogura, T.; Yamasaki, Y.; et al. Direct and Instantaneous Observation of Intravenously Injected Substances Using Intravital Confocal Micro-Videography. *Biomed. Opt. Express* **2010**, *1*, 1209–1216.

41. Jain, R. K.; Stylianopoulos, T. Delivering Nanomedicine to Solid Tumors. *Nat. Rev. Clin. Oncol.* **2010**, *7*, 653–664.

42. Shimizu, K.; Higuchi, Y.; Kozu, Y.; Hashida, M.; Konishi, S. Development of a Suction Device for Stabilizing *in Vivo* Real-Time Imaging of Murine Tissues. *J. Biosci. Bioeng.* **2011**, *112*, 508–510.